THERMO-MECHANICAL ANALYSIS OF LINEAR WELDING STAGE IN FRICTION STIR WELDING
Influence of Welding Parameters

by

Darko M. VELJIĆ [a*], ***Marko P. RAKIN*** [b], ***Aleksandar S. SEDMAK*** [c], ***Nenad A. RADOVIĆ*** [b], ***Bojan I. MEDJO*** [b], ***Mihailo R. MRDAK*** [a], **and *Darko R. BAJIĆ*** [d]

[a] Innovation Center of the Faculty of Technology and Metallurgy, University of Belgrade, Belgrade, Serbia
[b] Faculty of Technology and Metallurgy, University of Belgrade, Belgrade, Serbia
[c] Faculty of Mechanical Engineering, University of Belgrade, Belgrade, Serbia
[d] Faculty of Mechanical Engineering University of Montenegro, Podgorica, Montenegro

Original scientific paper
https://doi.org/10.2298/TSCI210216186V

The influence of friction stir welding parameters on thermo-mechanical behavior of the material during welding is analyzed. An aluminum alloy is considered (Al 2024 T351), and different rotating and welding speeds are applied. The finite element model consists of the working plate (Al alloy), backing plate and welding tool. The influence of the welding conditions on material behavior is taken into account the application of the Johnson-Cook material model. The rotation speed of the tool affects the results. If increased, it contributes to an increase of friction-generated heat intensity. The other component of the generated heat, which stems from the plastic deformation of the material, is negligibly changed. When the welding speed, i.e. tool translation speed, is increased, the intensity of friction-generated heat decreases, while the heat generation due to plastic deforming is becoming more pronounced. Summed, this leads to rather small change of the total generation. The changes of the heat generation influence both the temperature field and reaction force. Also, the inadequate selection of welding parameters resulted in occurrence of the defects (pores) in the model.

Key words: *friction stir welding, welding speed, heat generation, welding tool rotation speed, finite element analysis*

Introduction

Advanced joining technologies are crucial for manufacturing of lightweight structures. An example is friction stir welding (FSW) process, which is increasingly used for welding of structures produced from aluminum alloys and other metals. The process itself does not require filler material or protective atmosphere. The work (welding) environment is cleaner, without harmful fumes, smoke, oduors, ultraviolet, and other harmful radiation. No special preparation of joining surfaces or edges is required. Low heat input enables minimal distortions and shrinkage, and minimal influence of the introduced heat on the phase transformations in the base metal. The FSW produces joints without hot cracks and porosities, which are typical side effects of the welding procedures based on melting.

[*] Corresponding author, e-mail: veljic.darko@gmail.com

Application of FSW is gaining more attention in different industries, like shipbuilding, aerospace, railway/road vehicle production*, etc.* The aluminum alloys are the most often subjected to FSW, including those with poor weldability, *e.g.* 7049A T652 [1]. However, other metallic materials/alloys can be joined as well: magnesium [2], titanium [3], copper [4], or steel. Also, it is possible to weld dissimilar metals – different Al alloys, but also completely different materials, *e.g.* Al alloy 2024-T3 and TiAl6V4 [5]. Particle reinforced composites, such as aluminum matrix composites, have also been joined by FSW, as shown in [6].

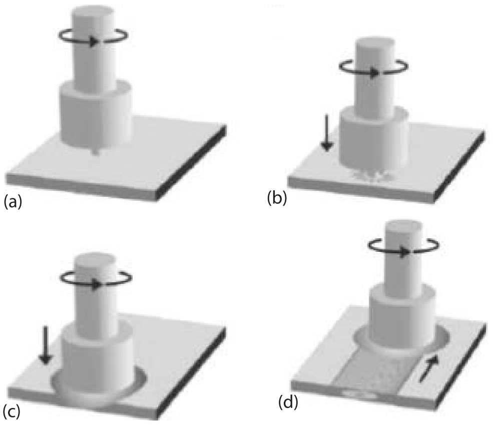

Figure 1. Sketch of FSW welding; (a) before contact, (b) tool pin in contact with plates, (c) tool shoulder in contact with plates, and (d) production of welded joint [7]

The stages of FSW are shown schematically in fig. 1, [7]. The process is initiated by plunging of the tool into the work pieces (tool rotation and vertical translation), while the welding stage starts after the thermo-mechanical conditions have been established. A review of equipment used for joining by FSW is shown in [8], and includes conventional machines, dedicated FSW machines, as well as industrial robots. Besides the machine itself, welding tools (which are non-consumable) affect the process; this refers to their shape/geometry [9] or state – whether the tool is worn or not [10].

Finite element simulations are generally very often used in literature to simulate the FSW process, *e.g.* [10-13], with a comprehensive review given in [14]. However, there are some interesting recent studies showing the application of other mathematical tools, such as cellular automaton model [2], or wavelet analysis [15] in modelling of this welding technique. Simulation of the joint formation is not the only area of application for numerical simulations they are also applied in fracture and failure analysis of FSW joints [16-18].

The FSW inevitably includes heat generation by two processes: the first one is the friction between the tool and the welded material, while the second is significant plastic deforming of the material. The welding depends on this heat generation, which is why the initial stage, plunge stage, has a key role. Namely, the thermo-mechanical conditions required for subsequent welding are established during this stage. Also, highest temperatures and strains are expected as the tool is plunged into the welded material. Therefore, special attention has been devoted to the plunge stage by the authors of the present study in [19, 20]. Also, previous works of the authors include determination of influence of material properties on both welding stages [19, 21] and analysis of the velocity fields in the material around the tool [22]. Comparison of numerically predicted temperature and force with the experimental findings is shown in [23] for Al alloy 2024 T3. It could be said that the findings of [23] represent a verification of the model used in this work, but performed on different material. Experimental examination of joints formed by application of different welding parameters on Al alloy 2024 T3 are conducted in [24]. The study [24] examines the effect of the welding parameters on tensile properties under static loading conditions, while impact loading is considered in [25]. The effect of heat input of FSW of AA 6061-T6 is studied in [26], while the heat input in general is studied in [27].

Here, the topic is analysis of the influence of welding parameters (welding speed and tool rotation speed) on heat generation, temperature, force and plastic strains during the linear welding stage of the Al alloy 2024 T351, by application of numerical analysis, *i.e.* finite element modelling. Also, some special cases with (deliberately) inadequate choice of welding parameters are considered, and the weld defects (pores) are predicted in such models.

Material properties

The base metal considered in this work is aluminum alloy EN AW 2024 T351. The material properties of this alloy were used in previous authors' works dealing with different aspects of FSW, such as [21, 22, 28], and are repeated in tab. 1.

Table 1. Properties of aluminum alloy 2024 T351 [29]

Material properties	Value
Young's modulus, E [GPa]	73.1
Poisson´s ratio, υ [–]	0.33
0.2% Yield strength, $R_{p0.2}$ [MPa]	324
Tensile strength, R_m [MPa]	469
Elongation at fracture, A_5 [%]	20
Thermal conductivity, k [Wm^{-1} °C^{-1}]	121
Coefficient of thermal expansion, α [°C^{-1}]	$24.7\cdot10^{-6}$
Mass density, ρ [kg m^{-3}]	2770
Specific heat capacity, c_p [Jkg^{-1} °C^{-1}]	875

Finite element modelling

Numerical model which is used for analysis of heat generation during welding is shown in fig. 2. Software package SIMULIA ABAQUS is applied [30]. As shown in the figure, it consists of three parts: the plate being welded, the welding tool with cylindrical pin, and the backing plate. The model is described in [21-23, 28], while only some main details and fig. 2 are given here.

Hexahedral finite elements C3D8RT are used, *i.e.* coupled thermo-mechanical elements with linear interpolation of displacement/temperature and reduced integration order, [30]. There are ten elements along the thickness (as shown in fig. 2, zoomed detail), in order to capture the change of thermo-mechanical quantities in this direction. As for the backing plate and the welding tool, they are considered as rigid bodies. Tool pin has cylindrical shape with diameter 6 mm, while tool shoulder diameter is 18 mm. It should be mentioned that the tool pin in this numerical study does not have a thread, which represents a simplification (often made in the literature) because the threaded pins are much more often used for actual welding. There are some recent studies where authors analyse the isolated influence of the thread, but the emphasis in this work is on comparison between the same models with different welding parameters.

Lagrange-Euler technique for mesh adjustment is applied. This includes the following boundary conditions: the material *flows* into and out of the model at the appropriate boundary surfaces. Figure 2 shows the positions of the two points used for tracking the change of temperature during the welding. The co-ordinates of these points are: T1 (17.5, 0, 3) and T2 (12, 0, 3). The co-ordinate system is aligned with the tool axis, and its origin is on the bottom of the working plate.

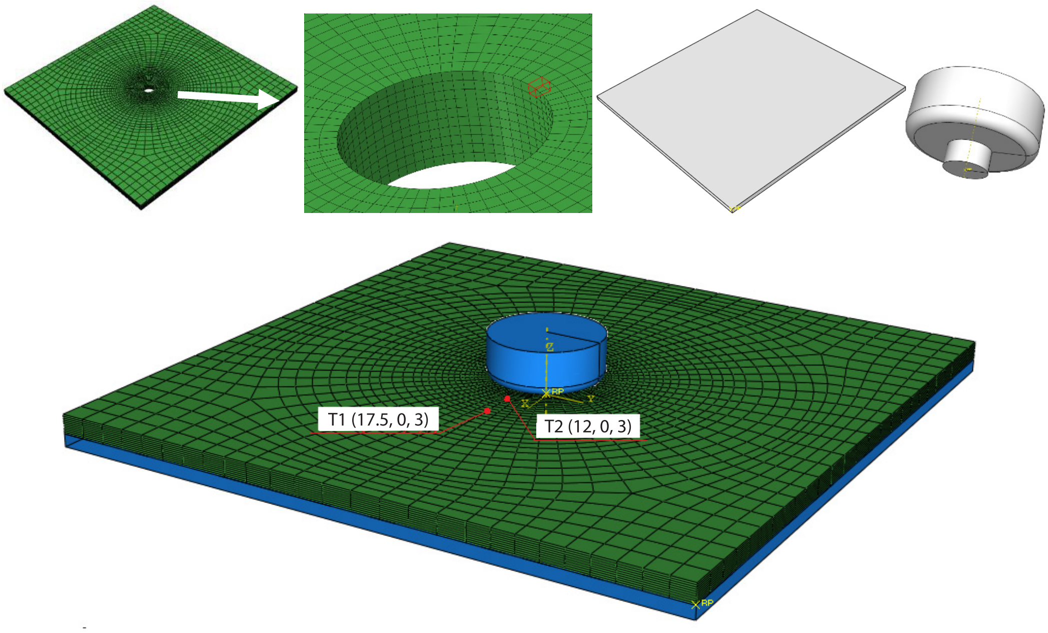

Figure 2. Finite element model; modified from [28]

Johnson-Cook elastic-plastic model

Dependence of the current yield stress σ_y [MPa] on temperature T [°C], plastic strain ε_p [–], and plastic strain rate $\dot{\varepsilon}_p$ [s^{-1}] is defined by Johnson-Cook material law [31]:

$$\sigma_y = \left[A + B(\varepsilon_p)^n \right] \left[1 + C\left(\frac{\dot{\varepsilon}_p}{\dot{\varepsilon}_o} \right) \right] \left[1 - \left(\frac{T - T_{\text{room}}}{T_{\text{melt}} - T_{\text{room}}} \right)^m \right] \tag{1}$$

where T_{room} = 20 °C is the ambient temperature, while $A, B, C, n, T_{\text{melt}}, T_{\text{room}}$, and m are Johnson-Cook material/test constants. For the considered alloy (Al 2024 T351): A = 265 MPa, B = 426 MPa, n = 0.34, m = 1, and C = 0.015, [32]. Solidus temperature T_{melt} is 502 °C.

Heat transfer model

Energy balance related to heat transfer analysis is described by the Fourier law. The same approach (including the parameters in the rest of this subsection) was used in previous authors' works for this alloy or Al 2024 T_3, *e.g.* [21-23, 28], also together with Johnson-Cook material model. Here, we will mention the applied expressions for heat generation, because it is one of the main concerns in this work. Equation (2) shows the total heat flux $\dot{q}$ [Js^{-1}], obtained as the sum of the following components:

– heat flux due to the shear plastic strain in the zone around the tool shoulder and tip $\dot{q}_p$ [Js^{-1}] and
– (heat flux due to the friction which happens during shearing between the tool and the plate $\dot{q}_f$ [Js^{-1}]:

$$\dot{q} = \dot{q}_p + \dot{q}_f = \eta\tau\dot{\varepsilon}_p + \mu p\dot{\gamma} \tag{2}$$

In this expression, the first component of the heat flux depends on: factor of conversion of mechanical to thermal energy, η [–], (applied value: 0.9, in accordance with [33]), shear stress, τ [MPa], and plastic strain. As shown previously, plastic strain also exists in the material model for mechanical behaviour, eq. (1). The heat flux due to the friction, *i.e.* the second component of the heat flux, is calculated from the friction coefficient, μ [–], contact pressure, p [MPa], and slip rate, $\dot{\gamma}$ [mms^{-1}]. At the contact surface between the working plate and the tool, 90% of the generated heat is transferred to the plate (*i.e.* to the welded material) and 10% is taken away by the tool.

As mentioned previously, the backing plate is modelled as the rigid body. Also, it has no thermal degrees of freedom. Therefore, heat transfer which occurs through this plate is simulated by a high value of the heat transfer coefficient defined at the bottom surface of the welding plate –h = 3000 W/m^2 °C, [34]. As for the surfaces of the welding plate which are in contact with the surrounding, *i.e.* air at room temperature, the value of this coefficient is 10 W/m^2 °C [21, 23, 33]. For definition of contact between the material and the tool, it is necessary to define the friction coefficient value: μ = 0.3.

Results and discussion

In this section, the results obtained by varying the welding speed and tool rotation speed are shown. Also, the effects of the inadequate selection of welding parameters are shown. It should be emphasised that the results presented here are numerical. Experimental verification of this numerical model is shown on the alloy Al 2024 in T3 condition in [23], where temperature and reaction force are compared with the experimentally measured values during the process.

Welding speed effect

Figure 3(a) shows the change of the heat generation intensity during the welding. In this diagram, both components of heat generation are shown (from friction and from significant plastic deformation), as well as total amount. All these quantities are presented for two different welding speeds, in order to assess the influence of this welding parameter. From fig. 3(a), it can be seen that the welding speed increase, with a constant tool rotation speed, causes decrease of friction heat generation and increase of deformation-generated component. However, total change is rather small. Actually, higher welding speeds cause the tool to interact with less-

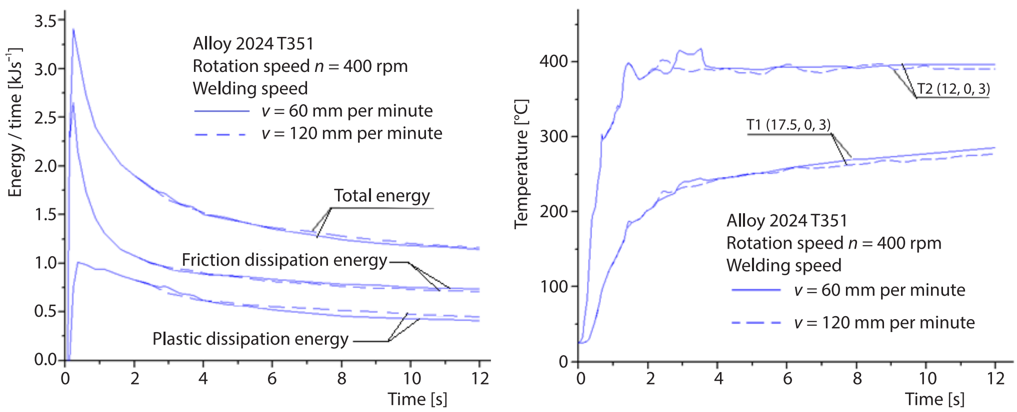

Figure 3. Heat generated (a) and temperature change (b) during the FSW

heated (insufficiently heated) material more quickly. Then the material will show an increased resistance to deformation and therefore, a larger amount of heat is generated due to plastic deforming. Since the working temperature is reached near the tool tip, the influence of friction is less pronounced and friction-generated heat amount is decreased. Figure 3(b) shows the temperatures in two defined points (T1 and T2, fig. 2) during the welding process. The welding speed does not have a pronounced influence, neither in the area close to the tool tip (T2), nor further from it (T1). This can be regarded as a consequence of the previous result - the speed does not have a significant influence on the total generated heat when near-optimal welding parameters are applied.

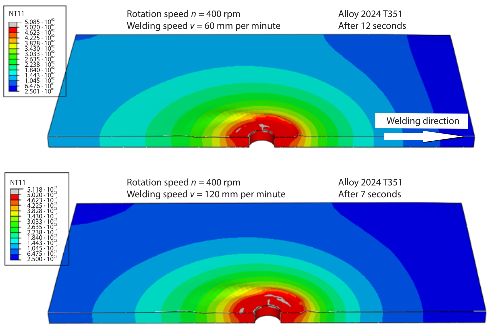

Figure 4. Temperature distributions for the same weld length and different welding speed

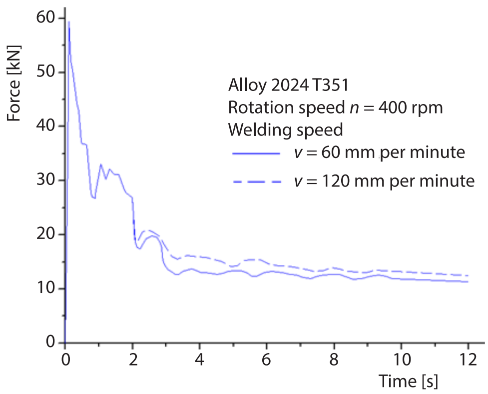

Figure 5. Force in vertical direction during FSW

The temperature fields in fig. 4 are shown for two welding speeds, but for this comparison the weld length obtained by these speeds is the same. Of course, this means that more time is needed to achieve this length if the welding speed is lower. For the tool with 120 mm per minute translation speed, 7 seconds was needed to reach this state, while 12 seconds was needed for the tool translation speed 60 mm per minute. In both cases, tool plunge stage had the same duration - two seconds. For the same path, the plate welded at lower speed is more intensively heated outside the welding zone. This difference can also be seen in fig. 3, if temperature at the position T1 is considered.

As a consequence of higher resistance to tool movement through the material, higher welding speeds cause higher force value in vertical direction, fig. 5.

Tool rotation speed effect

If we now apply different tool rotation speeds, maintaining the welding speed unchanged, it is determined that the rotation speed increase leads to an increase of friction-generated heat intensity. The intensity of the other component, deformation-generated, is changed negligibly (except in the first 3 seconds), fig. 6(a). Actually, the increase of rotation speed increases so-called tool slip rate-this quantity is actually relative velocity (when tool movement is observed relative to the material, *i.e.* plate), which makes the friction and heat generation by friction more intensive.

Due to the increase of total heat generation as the tool rotation speed increases, higher temperature values are observed both close to the welding tool and further from it – positions T1 and T2 in fig. 6(b). Temperature values in the narrower welding zone, close to the tool pin, do not change after the first few seconds, since they have already reached their maximum.

The distribution of temperature is given in fig. 7 where cross-sections are shown and welding direction is from left to right. Two fields are obtained, for the tool rotation speeds 400 rpm and 447 rpm. Welding speed was held constant for both cases – 60 mm per minute. A

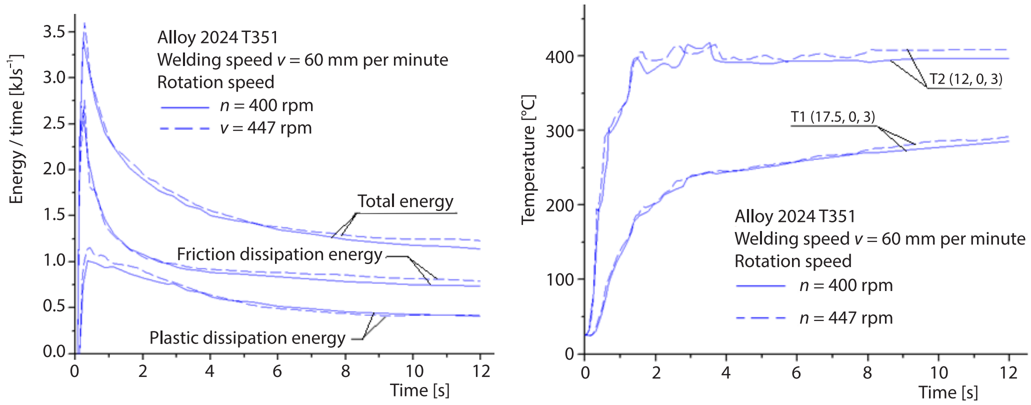

Figure 6. Heat generated (a) and temperature change (b) during the FSW – tool rotation speed effect

small difference between the two fields, caused primarily by change of the friction-generated heat intensity, can be noticed. From fig. 6(a), it has been concluded that the other component, deformation-induced heat generation, almost does not change with the increase of the tool rotation speed.

Comparison of the reaction forces of the material for different tool rotation speeds are shown in fig. 8. For the higher rotation speed (447 rpm), the material around the tool tip and shoulder is more intensively heated. Therefore, the reaction force in vertical direction (*i.e.* material resistance to deformation) will be lower, fig. 8.

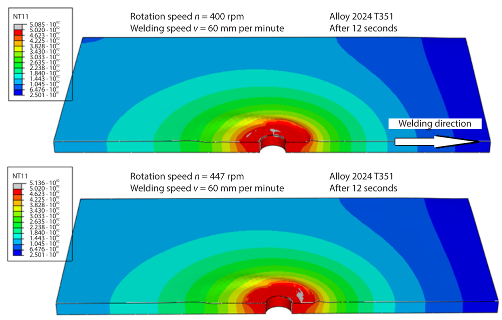

Figure 7. Temperature field after 12 seconds of FSW – tool rotation speed effect

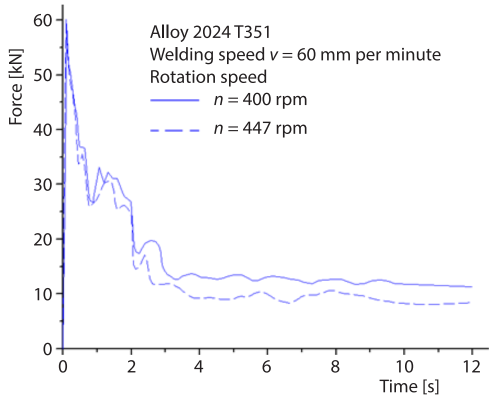

Figure 8. Force in vertical direction during FSW – tool rotation speed effect

Numerical results for parameters set outside the optimal range

When welding parameters are outside the optimal ranges (*e.g.* too high welding speed in fig. 9 or too low tool rotation speed in fig. 10), the generation of heat in the working plate is insufficient. As a consequence, the material is not sufficiently plastic, and the tool does not convey sufficient amount of material from one side of the weld (retreating) to the other (advancing). Such behaviour leads to formation of defects in the shape of voids, marked in figs. 9-12 by arrows, in the regions with low material velocity. It should be noted that tracking the exact shape and/or evolution of a void in the material would probably require some more advanced technique. However, its appearance is an important indicator that the selected FSW parameters are not adequate – such combinations lead to void formation, or at least to a significant decrease of mechanical properties of the joint.

In the numerical models with the temperature field distribution, it can be observed that the error has occurred. In fig. 9, it happens during the first second of the welding, while in fig. 10 the defect emerges in the third second.

The aforementioned problem can also be viewed by considering the flow rates of the material being welded, figs. 11 and 12. If the fields of the flow rate are analysed, it is visible that the flow rate in the weld root is minimal on the advancing side, *i.e.* the material transfer is insufficient. This corresponds with the previous two figures (note: different cross-section planes are used in figs. 11 and 12 when compared with previous two figures, which can be seen by the marked welding direction).

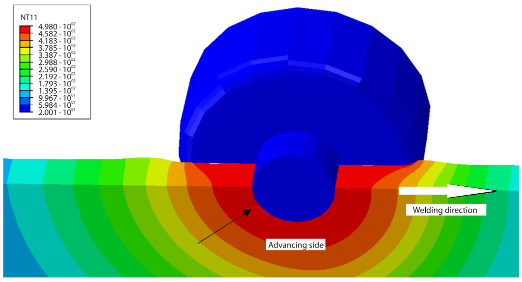

Figure 9. Void in the weld root – advancing side; *n* = 400 rpm, *v* = 240 mm per minute

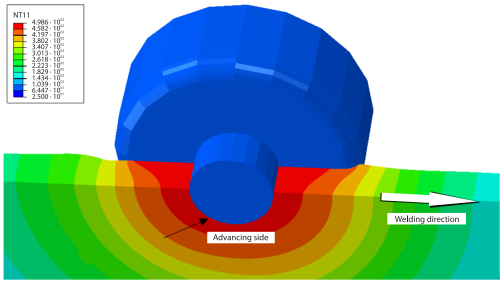

Figure 10. Void in the weld root – advancing side; *n* = 200 rpm, *v* = 60 mm per minute

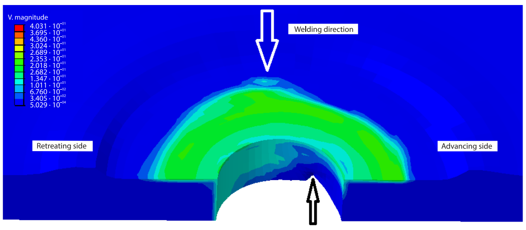

Figure 11. Material flow rate field; *n* = 400 rpm, *v* = 240 mm per minute

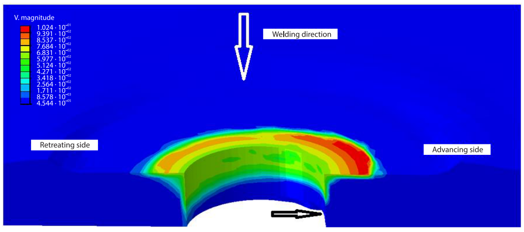

Figure 12. Material flow rate field; *n* = 200 rpm, *v* = 60 mm per minute

The results shown in this work capture the influence of the welding parameters on the thermo-mechanical quantities, primarily temperature, plastic strain, force and heat generation. Also, appearance of FSW defects (voids) for inappropriate values of the welding speed and/or tool rotation speed is predicted. In the studies [20, 21], the effect of difference of material properties on the similar set of thermo-mechanical quantities is analysed both during linear welding [21] and plunge [20] stage. The alloy 2024 T351 was one of the materials considered in these works, but with a single set of welding parameters, without variations which are applied here.

Conclusions

The main conclusions are given. As mentioned previously, they are based solely on numerical results and the model has previously been verified by authors on the Al alloy 2024 in T3 state.

- Increase of the welding speed leads to a decrease of friction-generated heat intensity and increase the generation of plastic deformation-generated heat. Total change of heat generation is negligible.
- Higher welding speeds lead to higher forces in vertical direction; this is caused by more pronounced resistance to tool movement through the material.
- When the tool rotates with increased speed, an increase of the friction-generated heat intensity is observed, while the other component of heat (caused by plastic deformation) is changed negligibly. Therefore, total heat generation is increased.
- The force in vertical direction is lower if the tool rotation speed is increased. The material resistance is less pronounced in this case, due to more intensive heating.
- Application of numerical modelling can be successful in assessment of the optimal values of the FSW parameters, thus decreasing the time and costs of the experimental examinations. Also, another important point is presented here: it can capture the formation of the defects due to inadequate welding parameters. Even though the exact shape and development dynamics of these defects might require some more advanced modelling strategy, their appearance in the models is an important indicator that insufficient properties (strength, ductility, *etc.*) of the joint will be obtained in these cases.

In the future work, we will attempt to also verify some of the results on the alloy 2024 T351, especially to check the prediction of the consequences of inadequate parameters selection (deterioration of joint properties).

Acknowledgment

This work was supported by the Ministry of Education, Science and Technological Development of the Republic of Serbia (Contracts No. 451-03-9/2021-14/200287, 451-03-9/2021-14/200135).

Nomenclature

n_{rot} – rotation speed of the tool, [rpm]
$\dot{q}$ – rate of total heat generation, [Js^{-1}]
$\dot{q}_f$ – rate of frictional heat generation, [Js^{-1}]
$\dot{q}_p$ – rate of heat generation due to plastic deformation, [Js^{-1}]
v – welding speed, [mms^{-1}]

Greek symbol

$\dot{\varepsilon}_p$ – equivalent plastic strain rate, [s^{-1}]

References

[1] Perović, M., *et al.*, Friction-Stir Welding of High-Strength Aluminum Alloys and a Numerical Simulation of the Plunge Stage, *Materials and Technologies*, *46* (2012), 3, pp. 105-111
[2] Akbari, M., *et al.*, A Cellular Automaton Model for Microstructural Simulation of Friction Stir Welded AZ91 Magnesium Alloy, *Modelling and Simulation in Materials Science and Engineering*, *24* (2016), 3, 035012
[3] Lauro, A., Friction Stir Welding of Titanium Alloys, *Welding International*, *26* (2012), 1, pp. 8-21
[4] Hwang, Y. M., *et al.*, Experimental Study on Friction Stir Welding of Copper Metals, *Journal of Materials Processing Technology*, *210* (2010), 12, pp. 1667-1672
[5] Dressler, U., *et al.*, Friction Stir Welding of Titanium Alloy TiAl6V4 to Aluminum Alloy AA2024-T3, *Materials Science and Engineering A*, *526* (2009), 1-2, pp. 113-117
[6] Salih, O., *et al.*, A Review of Friction Stir Welding of Aluminum Matrix Composites, *Materials and Design*, *86* (2015), Dec., pp. 61-71
[7] Mahoney, M.W., *et al.*, High Strain Rate Superplasticity in Thick Section 7050 Aluminum Created by Friction Stir Processing, *Proceedings*, 3rd International Symposium on Friction Stir Welding, Kobe, Japan, 2001
[8] Mendes, N., *et al.*, Machines and Control Systems for Friction Stir Welding: A Review, *Materials and Design*, *90* (2016), Jan., pp. 256-265

[9] Radisavljević, I., *et al.*, Influence of Pin Geometry on Mechanical and Structural Properties of Butt Friction Stir Welded 2024-T351 Aluminum Alloy, *Chemical Industry*, *69* (2015), 3, pp. 323-330
[10] Hasan, A. F., *et al*., A Numerical Comparison of the Flow Behaviour in Friction Stir Welding (FSW) Using Unworn and Worn Tool Geometries, *Materials and Design*, *87* (2015), Dec., pp. 1037-1046
[11] Chen, C. M., Kovačević, R., Finite Element Modelling of Friction Stir Welding – Thermal and Thermomechanical Analysis, *International Journal of Machine Tools & Manufacture*, *43* (2003), 13, pp. 1319-1326
[12] Mijajlović, M., *et al.*, Numerical Simulation of Friction Stir Welding, *Thermal Science*, *18* (2014), 3, pp. 967-978
[13] Zahaf, S., *et al.*, Optimization of FSW Welding Parameters on Maximal Temperature, von Mises and Residual Stresses, and Equivalent Plastic Deformation applied to a 6061 Aluminum Alloy, *Structural Integrity and Life*, *19* (2019), 3, pp. 195-209
[14] He, X., *et al*., A Review of Numerical Analysis of Friction Stir Welding, *Progress in Materials Science*, *65* (2014), Aug., pp. 1-66
[15] Das, B., *et al*., Weld Quality Prediction in Friction Stir Welding using Wavelet Analysis, *International Journal of Advanced Manufacturing Technology*, *89* (2017), 1, pp. 711-725
[16] Sun, G., *et al*., Fatigue Experimental Analysis and Numerical Simulation of FSW Joints for 2219 Al-Cu Alloy, *Fatigue and Fracture of Engineering Materials and Structures*, *38* (2015), 4, pp. 445-455
[17] Živojinović, D., *et al*., Crack Growth Analysis in Friction Stir Welded Joint Zones using Extended Finite Element Method, *Structural Integrity and Life*, *13* (2013), 3, pp. 179-188
[18] Đurđević, A., *et al*., Numerical Simulation of Fatigue Crack Propagation in Friction Stir Welded Joint Made of Al 2024-T351 Alloy, *Engineering Failure Analysis*, *58* (2015) Part 2, pp. 477-484
[19] Veljić, D., *et al.*, Heat Generation During Plunge Stage in Friction Stir Welding, *Thermal Science*, *17* (2013), 2, pp. 489-496
[20] Veljić, D., *et al*., Analysis of the Tool Plunge in Friction Stir Welding – Comparison of Aluminum Alloys 2024 T3 and 2024 T351, *Thermal Science*, *20* (2016), 1, pp. 247-254
[21] Veljić, D., *et al*., Temperature Fields in Linear Stage of Friction Stir Welding – Effect of Different Material Properties, *Thermal Science*, *23* (2019), 6B, pp. 3985-3992
[22] Veljić, D., *et al*., Influence of Material Velocity on Heat Generation during Linear Welding Stage of Friction Stir Welding, *Thermal Science*, *23* (2016), 5, pp. 1693-1701
[23] Veljić, D., *et al*., Experimental and Numerical Thermo-Mechanical Analysis of Friction Stir Welding of High-Strength Aluminum Alloy, *Thermal Science*, *17* (2013), Suppl. 1, pp. S28-S37
[24] Eramah, A., *et al*., Influence of Friction Stir Welding Parameters on Properties of 2024 T3 Aluminum Alloy Joints, *Thermal Science*, *18* (2014), Suppl. 1, pp. S21-S27
[25] Eramah, A., *et al*., Impact Fracture Response of Friction Stir Welded Al-Mg Alloy, *Structural Integrity and Life*, *13* (2013), 3, pp. 171-177
[26] Sedmak, A., *et al*., Heat Input Effect of Friction Stir Welding on Aluminum Alloy AA 6061-T6 Welded Joint, *Thermal Science*, *20* (2016), 2, pp. 637-641
[27] Ivanović, I., *et al*., Numerical Study of Transient 3-D Heat Conduction Problem with a Moving Heat Source, *Thermal Science*, *15* (2011), 1, pp. 257-266
[28] Veljić, D., *et al*., A Coupled Thermo-Mechanical Model of Friction Stir Welding, *Thermal Science*, *16* (2012), 2, pp. 527-534
[29] ***, ASM International Aluminum 2024-T351 Data Sheet
[30] ***, Dassault Systemes, Abaqus Analysis Manual, 2012
[31] Johnson, G. R., Cook, W. H., A Constitutive Model and Data for Metals Subjected to Large Strains, High Rates and High Temperatures, *Proceedings*, 7th International Symposium on Ballistics, The Hague, The Netherlands, 1983, pp. 541-547
[32] Lesuer, D. R., Experimental Investigations of Material Models for Ti-6Al-4V Titanium and 2024-T3 Aluminum, Final Report, Department of Transportation, Washington DC, USA, 2000
[33] Schmidt, H., Hattel, J., A Local Model for the Thermomechanical Conditions in Friction Stir Welding, *Modelling & Simulation in Materials Science and Engineering*, *13* (2005), 1, pp. 77-93
[34] Park, K., Development and Analysis of Ultrasonic Assisted Friction Stir Welding Process, Ph. D. thesis, University of Michigan, Ann Arbor, Mich., USA, 2009

Paper submitted: February 16, 2021
Paper revised: April 30, 2021
Paper accepted: May 5, 2021